Title page

Title:

Decoy-resistant IL-18 reshapes the tumor microenvironment and enhances rejection by anti-CTLA-4 in renal cell carcinoma

Authors: David A. Schoenfeld[1], Dijana Djureinovic[1], David G. Su[2], Lin Zhang[1], Benjamin Y. Lu[1], Larisa Kamga[3], Jacqueline E. Mann[1], John Huck[4], Michael Hurwitz[1], David A. Braun[1], Lucia Jilaveanu[1], Aaron Ring[5*±], Harriet M. Kluger[1*±]

Affiliations:

[1]Section of Medical Oncology, Yale School of Medicine; New Haven, Connecticut, USA.

[2]Section of Surgery, Yale School of Medicine; New Haven, Connecticut, USA.

[3]Department of Internal Medicine, Emory University School of Medicine; Atlanta, Georgia, USA.

[4]Department of Immunobiology, Yale School of Medicine; New Haven, Connecticut, USA.

[5]Immunotherapy Integrated Research Center, Fred Hutchinson Cancer Center; Seattle, Washington, USA.

*Corresponding authors. Harriet Kluger – 333 Cedar Street, PO Box 208028, New Haven, CT 06520; (203) 200-6622; Email: harriet.kluger@yale.edu. Aaron Ring – 1241 Eastlake Ave E, S3-204, Seattle, WA 98102; (206) 667-5001; aaronring@fredutch.org.

±The last two authors contributed equally to this work.

Conflicts of interest:

MH reports advisory boards for: Affini-T, Exelixis, Janssen, CRISPR Therapeutics, Pliant, Regeneron, TScan. Research for: AstraZeneca, Iovance. Other: Arvinas, Faeth.

DAB reports advisory board fees from Exelixis, AVEO, Eisai, and Elephas, equity in Elephas, Fortress Biotech (subsidiary) and CurIOS Therapeutics, consulting / personal fees from Cancer Expert Now, Adnovate Strategies, MDedge, CancerNetwork, Catenion, OncLive, Cello Health BioConsulting, PWW Consulting, Haymarket Medical Network, Aptitude Health, ASCO Post/Harborside, Targeted Oncology, Merck, Pfizer, MedScape, Accolade 2nd.MD, DLA Piper, AbbVie, Compugen, Link Cell Therapies, Scholar Rock, NeoMorph and research support from Exelixis and AstraZeneca, outside of the submitted work.

AR is the co-inventor of patents describing DR-18 and Founder and Director of Simcha Therapeutics, the commercial licensee of DR-18.

HMK reports institutional Research Grants (to the institution) from Merck, Bristol-Myers Squibb; Apexigen, and personal fees from Iovance, Merck, Chemocentryx, Bristol-Myers Squibb, Signatero, Gigagen, GI reviewers, Pliant Therapeutics, Esai, Invox, and Wherewolf.

The rest of the authors declare that they have no competing interests.

Abstract:

The cytokine interleukin-18 (IL-18) has immunostimulatory effects but is negatively regulated by a secreted binding protein, IL-18BP, that limits IL-18's anti-cancer efficacy. A "decoy-resistant" form of IL-18 (DR-18), that avoids sequestration by IL-18BP while maintaining its immunostimulatory potential, has recently been developed. Here, we investigated the therapeutic potential of DR-18 in renal cell carcinoma (RCC). Using pan-tumor transcriptomic data, we found that clear cell RCC had among the highest expression of IL-18 receptor subunits and *IL18BP* of tumor types in the database. In samples from RCC patients treated with immune checkpoint inhibitors, IL-18BP protein expression increased in the tumor microenvironment and circulating in plasma in non-responding patients and decreased in the majority of responding patients. We used immunocompetent RCC murine models to assess the efficacy of DR-18 in combination with single- and dual-agent anti-PD-1 and anti-CTLA-4. In contrast to preclinical models of other tumor types, in RCC models DR-18 enhanced the activity of anti-CTLA-4 but not anti-PD-1 treatment. This activity correlated with intra-tumoral enrichment and clonal expansion of effector $CD8^+$ T cells, decreased regulatory T cell levels, and enrichment of pro-inflammatory, anti-tumor myeloid cell populations. Our findings support further clinical investigation of the combination of DR-18 and anti-CTLA-4 in RCC.

Main Text:

INTRODUCTION

In recent years, the treatment paradigm for advanced renal cell carcinoma (aRCC) has shifted, with the emergence of immune checkpoint inhibitors (ICIs) that target CTLA-4 and PD-1, and newer-generation vascular endothelial growth factor receptor (VEGFR)-targeting tyrosine kinase inhibitors (TKIs). Combination regimens of dual ICIs targeting CTLA-4 and PD-1, or anti-PD-1 plus a TKI, have significantly extended overall survival compared to previous therapies (1, 2, 3, 4). Still, a sizable proportion of patients do not respond to front-line therapy, and among initial responders, responses are usually transient (5). There is substantial need for novel therapeutic approaches in RCC beyond traditional ICIs. Given the demonstrated immune responsiveness of RCC, new immunomodulatory agents represent a promising area for investigation (6).

Cytokine-based therapies represent one such approach. High-dose interleukin-2 (IL-2) and interferon (IFN)α have been used for decades in aRCC, albeit with low response rates (7). Other cytokine-based therapies, including IL-12, IL-15, and IL-21, are being explored (7). IL-18 is another potential anti-cancer cytokine. A member of the IL-1 cytokine family, IL-18 can stimulate innate lymphocytes and activate antigen-experienced T cells and is a potent inducer of IFNγ (8). Due to its immunostimulatory effects, recombinant IL-18 was previously tested in early-phase clinical trials, and while it was safe and well-tolerated, it lacked efficacy in melanoma (9, 10). However, IL-18 is negatively regulated by a secreted protein (IL-18BP) that binds to IL-18 with high affinity and thus prevents its interaction with the IL-18 receptor (11). Levels of IL-18BP increased in response to administration of recombinant IL-18, suggesting that IL-18BP may have abrogated maximal activity of IL-18 therapy (9).

A recent study demonstrated that IL-18BP is highly expressed in various cancers, including clear cell RCC (ccRCC), and that it functions as a secreted immune checkpoint in cancer (12). Directed evolution was used to engineer a modified version of IL-18, termed "decoy-resistant" or DR-18, which avoids neutralization by IL-18BP while still maintaining its immune cell stimulating potential. DR-18 exerted potent anti-tumor effects in mouse models of melanoma and colon cancer by remodeling the immune tumor microenvironment (TME) and activating antigen-specific $CD8^+$ tumor infiltrating lymphocytes (TILs), which were sufficient to induce anti-tumor responses. Anti-PD-1 enhanced the activity of DR-18 in the initial models tested. DR-18 also inhibited tumor growth in MHC class I-deficient tumors, a major mechanism of ICI resistance, through natural killer (NK) cell activity. DR-18 thus represents a promising therapeutic agent with the potential to synergize with ICIs and have activity in ICI-resistant settings. Accordingly, the first-in-human trial of the human version of DR-18 is currently underway to evaluate safety, pharmacokinetics, pharmacodynamics, and clinical activity in patients with relapsed or refractory solid tumors (NCT04787042).

Based on these preclinical data, the particularly high expression of *IL18BP* in ccRCC (12), and the demonstrated responsiveness of RCC to ICIs and other cytokine-based immunotherapies, we hypothesized that IL-18 could be an effective cytokine for treating aRCC. Herein, we investigated IL-18BP and the IL-18 receptor in RCC patient samples and determined the anti-tumor activity of DR-18 in RCC murine models and the combined effects with different ICIs.

RESULTS

ccRCC has high expression of IL-18 receptor subunits (*IL18R1* and *IL18RAP*) and *IL18BP*

We employed The Cancer Genome Atlas (TCGA) PanCancer data to determine mRNA expression of IL-18 receptor subunits (*IL18R1* and *IL18RAP*) and *IL18BP* in RCC. ccRCC has among the highest expression of both IL-18 receptor subunits and *IL18BP* relative to 29 other cancer types (Figure 1A and Supplemental Figure S1A). Comparing across the three most common RCC histologic subtypes (clear cell, papillary, and chromophobe), expression of IL-18 receptor subunits and *IL18BP* was highest in ccRCC and lowest in chromophobe RCC (Figure 1B and Supplemental Figure S1B). Higher *IL18BP* but not IL-18 receptor subunit expression was associated with higher disease stage in ccRCC (Figure 1C and Supplemental Figure S1C). Higher *IL18BP* expression in ccRCC was also associated with higher tumor grade, higher hypoxia signatures scores, and worse survival (Figure 1D and Supplemental Figure S1D-E). Transcriptional analysis revealed that ccRCC tumors with high *IL18BP* expression enrich for markers of cytokine/chemokine signaling, T cell activation, and neutrophil/granulocyte chemotaxis (Figure 1E-F and Supplemental Figure S2A, Supplemental Table 1). Numerous immune checkpoints were among the most significantly upregulated genes with high *IL18BP* expression, and *IL18BP* expression was highly correlated with *LAG3*, *TIGIT*, *PDCD1*, and *CTLA4* expression, as well as expression of the regulatory T cell (Treg) marker *FOXP3* and *CD4* (Supplemental Figure S2B and Supplemental Table 2). *IL18BP* and *IL18* levels were also significantly correlated, although to a lesser degree (Supplemental Figure S2C). Altogether, these findings suggest that the IL-18 – IL-18BP axis may play in an important role in shaping the TME in at least a subset of ccRCC tumors.

IL-18BP protein expression increases post-ICIs in non-responding RCC patients

We next quantified IL-18BP protein expression in the TME using a well-established method of quantitative immunofluorescence (qIF) employing tissue microarrays of human RCC samples (Supplemental Table 3) (13, 14). Representative histospot staining patterns are shown in Supplemental Figure S3A. IL-18BP was expressed in both primary RCC tumors and metastases, with lower expression in brain metastases (Supplemental Figure S3B). Among patients treated with ICI-based therapies (treatment regimens shown in Supplemental Table 3), higher IL-18BP expression was associated with worse overall survival (Figure 2A). IL-18BP levels also significantly increased post-immunotherapy in non-responding patients (stable or progressive disease) (Figure 2B).

To determine if these findings extended beyond the tumor microenvironment, we quantified circulating plasma levels of IL-18BP using ELISA in RCC patients pre- and post-treatment with ipilimumab and nivolumab (ipi + nivo) in the frontline setting (Supplemental Table 4). Patient-matched plasma IL-18BP levels did not significantly change with treatment (Figure 2C). However, when the patients were separated by response to ipi + nivo, a treatment effect was apparent: in responders (complete or partial responses), plasma IL-18BP levels did not significantly change with ipi + nivo, but they increased significantly in non-responders, consistent with the qIF data (Figure 2D-E and Supplemental Figure S3C). Notably, while plasma IL-18BP levels increased in 100% of non-responders post-treatment, they decreased in 67% of responders (Figure 2F). Further, we found that patients whose plasma IL-18BP levels decreased post-immunotherapy had longer progression-free survival (Figure 2G). We did not observe the same patterns with circulating plasma levels of IL-18. Patient-matched plasma IL-18 levels increased post-treatment with ipi + nivo but did so at equivalent levels between responders and non-responders (Supplemental Figure S3D-G). No differences in circulating IL-18 levels were

observed between responders and non-responders pre- or post-treatment, with nearly all patients having increased plasma IL-18 levels post-treatment (Supplemental Figure S3H). Interestingly, circulating IL-18 and IL-18BP levels were significantly correlated in responders, particularly pre-treatment, while levels were not correlated in non-responders (pre- or post-treatment) (Supplemental Figure S3I).

DR-18 in combination with anti-CTLA-4 demonstrates enhanced *in vivo* activity in RCC and melanoma murine models

Having seen that the IL-18 pathway may be primed for reactivation in ccRCC, we next performed tumor growth and survival analyses in two syngeneic, immunocompetent murine RCC models: Renca and RAG (15, 16). We tested DR-18 monotherapy and combination therapy with single- and dual-agent ICIs, including both anti-PD-1 and anti-CTLA-4 targeting antibodies (Figure 3A). In the Renca model, DR-18 monotherapy modestly inhibited tumor growth and prolonged survival, comparable to ICIs (Figure 3B-C and Supplemental Figure S4A). Interestingly, adding PD-1 blockade to DR-18 did not enhance efficacy whereas the addition of anti-CTLA-4 to DR-18 significantly increased anti-tumor effects. Triple-therapy (DR-18 + anti-PD-1 + anti-CTLA-4) did not further inhibit tumor growth or prolong survival compared to the doublet (DR-18 + anti-CTLA-4). The RAG model was more sensitive to ICIs but produced similar results, again showing a greater impact of anti-CTLA-4 than anti-PD-1 when combined with DR-18 (Figure 3D-E and Supplemental Figure S4B-D). Immune cell depletion studies in the Renca model demonstrated that $CD8^+$ T and NK cells, and IFNγ, but not $CD4^+$ T cells, are similarly required for activity of DR-18 + anti-CTLA-4 (Figure 3F). We conclude that DR-18 monotherapy

has modest activity in murine RCC models but the combination of DR-18 + anti-CTLA-4 may be particularly effective.

We then investigated whether the efficacy of DR-18 plus anti-CTLA-4 extended beyond RCC models. In the murine melanoma model YUMMER1.7, DR-18 was efficacious as a monotherapy and demonstrated added activity with anti-PD-1 (Supplemental Figure S4E-F) (12). DR-18 plus anti-PD-1 efficacy was comparable to dual-agent ICIs in YUMMER1.7 and was higher than in the RCC models. DR-18 plus anti-CTLA-4 was equally as effective as these regimens in the YUMMER1.7 model.

In the RAG and YUMMER1.7 models, where multiple mice treated with various drug regimens had complete tumor regression and prolonged responses, tumor rechallenge studies with twice the initial dose of tumor cells were performed. In all mice tested, no tumors grew out on rechallenge regardless of the initial treatment regimen, indicating prolonged anti-tumor memory responses.

DR-18 in combination with anti-CTLA-4 induces a broad inflammatory response

We then sought to understand how the combination of DR-18 and anti-CTLA-4 alters the mouse immune system. To start, we profiled circulating cytokines/chemokines in mice with Renca tumors after two different timepoints of treatment with single-agent or combination DR-18 + anti-CTLA-4 (Figure 4A). After the first treatment, DR-18-containing regimens produced increases in multiple inflammatory cytokines, including IFNγ, IP-10 (CXCL10), MIG (CXCL9), IL-5, G-CSF, and MCP-1 (CCL2) (Figure 4B-D). Increases in IFNγ, IP-10, and MIG were particularly pronounced with DR-18 + anti-CTLA-4 treatment (Figure 4C-D). Of note, IP-10 and MIG are known to be induced by IFNγ. After the third treatment, these and most of the other

cytokines/chemokines profiled were elevated in the DR-18 + anti-CTLA-4 treated mice, suggesting the induction of a broad inflammatory response by this point in the treatment course, including Th1, Th2, and Th17 programs.

Enrichment and clonal expansion of effector CD8$^+$ T cells with DR-18 plus anti-CTLA-4

To gain insight into global changes to the TME with DR-18, anti-CTLA-4 or the combination, we performed single-cell RNA and T cell receptor (TCR) sequencing (scRNA-seq and scTCR-seq) of Renca tumors with and without treatment (Figure 4A). A comparison of the proportion of different infiltrating immune cell types revealed largescale changes in granulocytes and macrophages/monocytes with DR-18 treatment (Figure 5A-B and Supplemental Figure S5A-D), reproducing prior findings ($P<0.0001$, control vs. each DR-18 containing regimen, Fisher's exact test) (12). Only the combination of DR-18 and anti-CTLA-4 led to higher relative CD4$^+$ and CD8$^+$ T cell infiltration compared to every other regimen ($P<0.0001$, Fisher's exact tests) (Figure 5B and Supplemental Figure S5D).

To probe tumor-infiltrating T cell population differences based on treatment groups, we performed differential abundance testing on the T cell subsets using Milo, which assigns cells to partially overlapping neighborhoods on a k-nearest neighbor graph and then groups neighborhoods (Figure 5C and Supplemental Figure S6A) (17). Comparing the most prominent enriched neighborhood group containing a substantial number of neighborhoods (#7) to the most de-enriched (#4) with combination treatment, we observed enrichment of numerous markers of CD8$^+$ T cell activation and cytolytic activity, as well as exhaustion markers, including *Cd8a, Tox, Klrd1, Klrc1*, *Ifng*, and the immune checkpoints *Tigit, Pdcd1, and Lag3* (Figure 5D-E and Supplemental Figure S6B). Similar analyses of other neighborhood groups revealed de-enrichment of Treg cells

(#1) and mild enrichment of an activated $CD4^+$ T cell population (#5) (Supplemental Figure S6C-E).

To verify these findings, we performed additional analysis on the T cell subsets. Unsupervised hierarchical clustering revealed an enriched population of activated $CD8^+$ T cells with combination treatment (cluster 0) (Supplemental Figure S7A-C). Semi-supervised analysis with well-annotated reference murine TIL markers similarly demonstrated enrichment of effector $CD8^+$ T cells (both precursor and terminally exhausted $CD8^+$ populations), as well as a concomitant decrease in $CD8^+$ and $CD4^+$ naïve-like populations, with the combination regimen (Supplemental Figure S7D-G). While treatment with DR-18 monotherapy elicited a relative increase in Treg cells, with the combination of DR-18 and anti-CTLA-4, the relative proportion of Treg cells remained stable (Supplemental Figure S7F-G). Focused analysis of immune checkpoint expression on T cells revealed strong induction of *Ctla4*, and to a lesser extent *Pdcd1* and *Tigit*, with DR-18 monotherapy, whereas there was stronger induction of *Pdcd1* and *Tigit* relative to *Ctla4* with DR-18 + anti-CTLA-4 (Supplemental Figure S8A).

Single-cell TCR analysis further demonstrated a greater degree of clonal expansion and loss of clonal diversity after treatment with the combination of DR-18 + anti-CTLA-4 relative to either monotherapy (Figure 5F-G and Supplemental Figure S8B-C). While no single clonotype was detected across all four treatment groups, a $CD8^+$ clonotype from the DR-18 monotherapy arm expanded to become a dominant effector $CD8^+$ clonotype in the combination arm (Supplemental Figure S8D-E).

Expansion of pro-inflammatory myeloid populations with DR-18 plus anti-CTLA-4

Given the importance of myeloid populations in immune modulation in RCC, we characterized changes to myeloid populations with DR-18, anti-CTLA-4, and the combination. Unsupervised hierarchal clustering of the monocyte/macrophage subsets suggested population shifts with drug treatment (Figure 6A and Supplemental Figure S9A). To phenotypically classify these clusters, we employed the classification system for murine tumor associated macrophages (TAMs) and tumor-infiltrating monocytes (TIMs) described in *Ma et al* (18). This analysis revealed reductions in pro-tumorigenic TAM subtypes, particularly the lipid-associated (LA)-TAMs, with DR-18 treatment, as well as increased infiltration of classical TIMs, traditionally associated with pro-inflammatory effects ($P<0.0001$, control vs. each DR-18 containing regimen, Fisher's exact test) (Figure 6B-C and Supplemental Figure S9B-C). The DR-18 + anti-CTLA-4 combination also led to the expansion of a TAM population compared to every other regimen ($P<0.0001$, Fisher's exact tests) defined by markers from multiple phenotypic subtypes, both pro-inflammatory and pro-tumorigenic (termed "Mixed TAMs"). This finding aligns with the concept that macrophages exist on a phenotypic and functional spectrum (18, 19, 20).

We had also observed increased infiltration of granulocytes after treatment with DR-18, either monotherapy or in combination with anti-CTLA-4, in accord with prior findings (Figure 5B) (12). We hypothesized that phenotypic shifts in granulocyte populations could also be occurring when the combination is given relative to monotherapy, given the difference in efficacy between the two treatments. Unsupervised hierarchal clustering of the granulocyte subsets indeed showed a divergence in granulocyte populations between DR-18 monotherapy and the combination with anti-CTLA-4 (Figure 6D and Supplemental Figure S9D). Differential gene expression analysis revealed enrichment of gene sets associated with type II interferon signaling and cytokines and inflammatory response in granulocytes from combination-treated tumors (Figure 6E-F).

Recent work has better defined the phenotypic and functional diversity of neutrophils in cancer, which can have both pro- and anti-tumorigenic roles (21, 22, 23, 24, 25). We applied one such classification system that has both human and mouse tumor relevance and has been functionally validated in mouse tumor models to our tumor infiltrating granulocyte population (Figure 6G-H and Supplemental Figure S9E-F) (21, 25). The relative proportions of the N1 and N2 neutrophil subtypes increased with DR-18 + anti-CTLA-4 treatment compared to every other regimen ($P<0.0001$, Fisher's exact tests). Of note, these subtypes had been previously identified and functionally validated as playing important roles in tumor control in response to immunotherapy, driven by IFNγ stimulation downstream of lymphocyte-myeloid cell crosstalk (21, 25). Ligand-receptor network analysis using NicheNet (26) indeed indicated that the neutrophils from DR-18 + anti-CTLA-4 treated tumors were stimulated by IFNγ produced by $CD8^+$ T cells (Supplemental Figure S10A).

We verified the findings from this semi-supervised analysis with unsupervised quantitative differential abundance and nearest neighbor clustering analysis using Milo, which showed high levels of enrichment of a neighborhood group (#4) with combination DR-18 + anti-CTLA-4 treatment that was overlapping with neutrophil subtype N2 and expressed high levels of interferon-response genes (Supplemental Figure S10B-F). Trajectory analysis showed neutrophils passing through intermediate subtypes before ultimately becoming N1 and then N2 subtypes, coinciding with the pathway to combination DR-18 plus anti-CTLA-4 treatment (Figure 6I).

DISCUSSION

In this study, we investigated the therapeutic potential of "decoy-resistant" IL-18 (DR-18) in RCC. We found that ccRCC tumors express high levels of both IL-18 receptor subunit

genes and the secreted blocking protein *IL18BP* relative to other cancer types. Further, an increase in IL-18BP protein expression with ICIs was associated with resistance to treatment in RCC, suggesting that IL-18BP might play a role in poor response to ICIs. Using murine models of RCC, we observed modest anti-tumor effects from DR-18 monotherapy. However, adding PD-1 blockade to DR-18 did not enhance efficacy whereas the addition of anti-CTLA-4 to DR-18 significantly increased anti-tumor effects. This activity correlated with proinflammatory immune microenvironment changes that support therapeutic efficacy.

Our human sample studies implicate circulating IL-18BP, and more specifically the change in IL-18BP from pre- to post-treatment, as a potential predictive biomarker for RCC patients treated with ICIs. We observed a significant increase in plasma IL-18BP protein levels after initiation of ICIs relative to baseline in non-responding patients only. Moreover, in a non-overlapping RCC patient cohort, we observed an increase in tumor IL-18BP protein levels by qIF, indicating that this is both a systemic and local phenomenon. Although our cohort sizes were small, an increase in circulating IL-18BP plasma levels with treatment was found in all eight non-responding patients treated with ipilimumab and nivolumab, while six of nine responding patients had a decrease in circulating IL-18BP. Of note, while these findings need to be verified in larger, independent RCC cohorts, measuring circulating IL-18BP plasma levels at baseline and on-treatment (e.g., after 3 cycles of treatment, as done here) would likely not be difficult to implement into clinical practice if indeed the sensitivity and specificity in larger cohorts remains high. It is unclear to what extent these findings extend outside of RCC and ipi + nivo treatment and requires further investigation.

In both syngeneic murine RCC models tested, we found that the combination of DR-18 plus anti-CTLA-4 had superior efficacy to either agent alone. This stood in contrast to the

combination of DR-18 plus anti-PD-1 in these models, which offered little additional benefit relative to each monotherapy. This finding in RCC models differed from the results seen previously in the mouse YUMMER1.7 melanoma model, where DR-18 + anti-PD-1 had increased anti-tumor effects (12), although in the YUMMER1.7 model enhanced activity was still seen with DR-18 + anti-CTLA-4. These results suggest that the optimal therapy to combine with DR-18 may vary based on tumor type and certain characteristics of the TME.

Single-cell transcriptomic analysis revealed more robust induction of *Ctla4* relative to *Pdcd1* on intratumoral T cells after 3 cycles of treatment with DR-18 monotherapy in the Renca model, offering a potential partial explanation for the superior efficacy of DR-18 + anti-CTLA-4 relative to DR-18 + anti-PD-1 in this model. Additionally, anti-PD-1 and anti-CTLA-4 immune checkpoint inhibitors are known to have distinct mechanisms of action, with anti-CTLA-4 agents more capable of activating and expanding T cells, particularly $CD4^+$ T cells, in the tumor draining lymph nodes, leading to increased trafficking of activated T cells into the tumor microenvironment (27, 28, 29, 30). Immune cell depletion experiments in the Renca model, however, showed that partial depletion of $CD4^+$ cells with a depleting antibody did not significantly alter the efficacy of DR-18 + anti-CTLA-4, suggesting that $CD4^+$ T cells may not be pivotal drivers of anti-tumor immunity in this particular situation or that smaller numbers of $CD4^+$ cells are sufficient to enhance $CD8^+$ activity, which appears to be critical. Additionally, the scRNA-seq T cell subset analysis did not show substantial expansion and activation of effector $CD4^+$ populations with DR-18 + anti-CTLA-4 but did indicate de-enrichment of Treg cells. Anti-CTLA-4 therapy is capable of depleting Treg cells in mouse tumor models and some human tumors, and while this is thought to be one of the major mechanisms of anti-CTLA-4 efficacy in mouse models, its role in human tumors is less clear (31, 32, 33, 34). The anti-CTLA-4 clone used in this study (9H10) is known to

deplete murine Treg cells (35). Further, tumors treated with DR-18 monotherapy had increased proportions of Treg cells relative to the other treatment groups (nearly twice as many), whereas Treg levels remained stable relative to control-treated tumors with DR-18 + anti-CTLA-4. Altogether, these findings suggest that one mechanism of enhanced efficacy of the combination of DR-18 and anti-CTLA-4 is the limitation of DR-18-induced Treg cell expansion by anti-CTLA-4, although additional studies are needed to unequivocally define the precise mechanisms, including the role of the tumor draining lymph node.

Myeloid populations, including macrophages and neutrophils, are important contributors to anti-tumor immunity, although they can have pro- and anti-tumorigenic roles (18). As seen previously (12), we observed shifts in macrophages/monocytes towards more pro-inflammatory, anti-tumor phenotypes with DR-18 treatment, changes that were more pronounced when combined with anti-CTLA-4. We also reproduced prior reports showing higher relative neutrophil infiltration with DR-18 (12). The rapid and robust increase in IP-10 and MIG levels with DR-18 treatment implicates these chemokines as possible mediators of this effect, as they are known neutrophil chemoattractants. Persistently high IFNγ stimulation could also explain the phenotypic shift in neutrophils towards an interferon-stimulated subtype with DR-18 + anti-CTLA-4. The phenotype of these neutrophils was highly overlapping with the N1 and N2 neutrophil subtypes recently identified as vital components of effective anti-tumor immunity in mouse tumor models (21, 25). Further studies are needed to determine if the neutrophil populations seen in this study play a similar role.

IL-18BP is highly expressed in numerous cancers, including ccRCC (12). While DR-18 has been engineered to avoid sequestration by IL-18BP to enable immune activation, alternative strategies exist to overcome IL-18BP inhibition and could also be investigated in combination with

CTLA-4 blockade. Examples of such alternative strategies include use of a decoy-to-the-decoy (36) or monoclonal antibodies targeting IL-18BP (37), both of which would have the effect of increasing endogenous IL-18 activity in the TME. These approaches have the potential of better tolerability, as they would theoretically limit their activity to areas of increased IL-18BP expression, such as the TME. However, as they rely on endogenous IL-18, they may also have lower efficacy and may not be effective for all tumor types or anatomic sites of disease, depending on patterns of IL-18 expression. Additionally, in some situations, IL-18 has demonstrated pro-tumorigenic effects (38), although this is thought to be dose- and context-dependent, in keeping with the pleiotropism that can characterize cytokines. In our studies and previous reports (12) (39), DR-18 has not displayed tumor-promoting activity. Expression of decoy-resistant IL-18 variants is also being utilized in adoptive cell therapies, including chimeric antigen receptor T cells, to potentiate anti-tumor effects, and has shown promising preclinical activity (40).

This study has several limitations. The predictive biomarker studies on IL-18BP relied on small, single-institution RCC cohorts. Further work in larger, multi-institution cohorts is needed to verify these findings. Additionally, although well-established murine RCC models, neither the Renca nor RAG lines mimic human RCC genetics. As a result, their clinical predictive value may be more limited. While the field was previously constrained by the lack of other syngeneic, immunocompetent murine models, recently a novel syngeneic murine RCC cell line, LVRCC67, was developed by engineering the loss of *Vhl*, *p53*, and *Rb1*, and overexpression of *c-myc* (41). Future studies should incorporate these and other novel models into preclinical testing.

Despite these caveats, the results of this study still strongly suggest that a combination of the human version of DR-18 with an anti-CTLA-4 agent may be an effective treatment option in RCC. Currently, the best treatment strategy at the time of progression with ICI-resistant RCC is

unclear. Various VEGF-pathway targeting drugs are commonly used, with response rates in the ~20-45% range, although with limited duration of responses and very few if any long-term responses (PFS of 6–12 months) (42, 43, 44, 45, 46, 47). The combination of atezolizumab, an anti-PD-L1 agent, with cabozantinib offered no additional benefit over cabozantinib alone in the ICI-resistant/refractory setting (48). Additionally, RCC patients treated with an anti-CTLA-4-containing regimen after non-response to an anti-PD1-containing regimen have overall response rates in the 4-15% range across historical studies (49, 50, 51, 52). Our human transcriptomic, qIF, and ELISA findings in RCC suggest that the IL-18 pathway may be poised for reactivation in RCC with an agent like DR-18 that can bypass the inhibitory protein IL-18BP, particularly in ICI-non-responding patients. Given these data, the efficacy of DR-18 and anti-CTLA-4 combined therapy in the models tested, including Renca, a relatively ICI-resistant model, and prior findings on DR-18 efficacy in the MHC-I deficient setting (12), a clinical trial exploring the safety and efficacy of DR-18 plus anti-CTLA-4 in ICI-resistant/refractory RCC should be considered, potentially exploring changes in IL-18BP levels in tumor and/or plasma to select patients.

METHODS

Sex as a biological variable:

For studies involving patient specimens, specimens from both male and female patients were included, reflecting the underlying sex ratio of RCC (roughly 2:1 male to female ratio). For the mouse studies, only male mice were used, as the mouse cancer cell lines used in this study derived from male mice only.

Patient specimens

Human plasma samples were collected at Yale University from patients with RCC treated with immune checkpoint inhibitor containing regimens. Samples used for analysis were collected at baseline (pre-treatment) and at the beginning of the third cycle of treatment for nearly all patients (approximately 6 weeks later). Patient and tumor characteristics, treatment responses, and timepoints of sample collection are noted in Supplemental Table 4. The study protocols were approved by the Institutional Review Board of Yale University and all patients provided written informed consent.

Mice

BALB/cJ-000651 and C57BL/6J-000664 mice were ordered from Jackson Laboratory and used in the indicated experiments. They were maintained in accordance with the guidelines from the Institutional Animal Care and Use Committee (IACUC). Experiments were performed in accordance with IACUC-approved protocols using and age-and gender-matched mice.

Cell lines

The following cell lines were used: Renca (ATCC, CRL-2947); RAG (ATCC, CCL-142); and YUMMER1.7 (Yale, M. Bosenberg) (53). Renca cells were cultured in RPMI-1640 (Corning, 10-040-CV) plus 10% fetal bovine serum (FBS) (Gibco, 16140-071), 1x MEM non-essential amino acids (Gibco, 11140-050), sodium pyruvate (1 mM) (Gibco, 11360-070), L-glutamine (2 mM) (Gibco, 25030-081), and 1x antibiotic-antimycotic (Gibco, 15240-062). RAG cells were

grown in Eagle's Minimum Essential Medium with 1.5 g/L sodium bicarbonate, non-essential amino acids, L-glutamine, and sodium pyruvate (Corning, 10-009-CV) plus 10% FBS and 1x antibiotic-antimycotic. YUMMER1.7 cells were cultured in DMEM/F12 with L-glutamine and 15 mM Hepes (Gibco, 11330-032) plus 10% FBS, 1x MEM non-essential amino acids, and 1x antibiotic-antimycotic. All cells were cultured at 37°C, 5% CO_2, and kept at low passage prior to mouse engraftment (< passage 10-12).

Mycoplasma testing was performed using the MycoAlert Mycoplasma Detection Kit (Lonza, LT07-318) – all cell lines tested negative.

Immunofluorescent staining

Two previously reported RCC tissue microarrays (TMAs) were used for IL-18BP quantitative immunofluorescent analysis: YTMA166, containing paired primary tumors and metastases; and YTMA-528, containing primary tumors and metastases, including brain metastases, from brain-metastases susceptible patients (13, 14, 54, 55, 56). The TMAs consisted of 0.6 mm cores spaced 0.8 mm apart. Two independent pathologists had reviewed and selected areas of tumor. Collection of patient specimens and clinical data was approved by the Yale University Institutional Review Board. Characteristics of the tumor specimens included for analysis are shown in Supplemental Table 3.

Immunofluorescent staining of the two TMA was performed as previously described (57) (58) . Briefly, 5 μm TMA sections mounted on glass slides were deparaffinized in xylene, rinsed in ethanol, and then boiled for 15 minutes in 6.5 mM citrate buffer (pH 6.0) for antigen retrieval. Slides were then incubated with methanol and 0.75% hydrogen peroxide, blocked with 0.3%

bovine serum albumin (BSA) in TBS, and incubated overnight at 4°C with anti-IL-18BP antibody (Invitrogen, PA5-116465) diluted 1:800 in 0.3% BSA/TBS. A signal amplification step was added using the secondary anti-rabbit EnVision antibody + HRP (Dako, K4003) and HRP-activated Cy5-tyramide (1:50; Akoya Biosciences, SAT705A001EA) following the manufacturer's protocol. HRP quenching was performed with 100 mM benzoic hydrazide + 50 mM hydrogen peroxide in PBS. Following washings, to create a tumor mask slides were incubated overnight at 4°C with anti-CA9 (1:1000; gift of Jan Zavada) and anti-cytokeratin (1:200; Dako, M3515) antibodies and streptavidin HRP (1:200; Sigma, S2438) in 0.3% BSA/TBS. Slides were washed and the signal was amplified using anti-mouse EnVision system + HRP (Dako K4001) and Cy3-Tyramide (1:50; Akoya Biosciences, SAT704A001EA). Slides were incubated for 20 minutes with 4,6-diamidino-2-phenylindole (DAPI) diluted at 1:300 and mounted with ProLong Gold Antifade Mountant (Invitrogen, P36931).

Multispectral image acquisition and quantitative determination of target expression:

Image acquisition and quantitative measurements were performed as previously described (57). The tumor mask was created from the CA9/cytokeratin signal through automated processing and thresholding and was used to distinguish tumor from stromal elements. A total tissue mask (tumor plus stroma) was created from the DAPI signal, which defined the nuclear compartment. A stromal compartment was created by subtracting the tumor mask from the total tissue mask. IL-18BP signal (total normalized signal intensity/area of the compartment) was quantified for the tumor and stromal compartments, and then summed for the total IL-18BP signal in the tumor microenvironment (tumor + stroma). Tumor spots were excluded if they contained insufficient tissue or abundant necrotic tissue, or significant artifacts.

ELISA

IL-18 and IL-18BP ELISAs were performed using the Human Total IL-18 DuoSet ELISA (R&D Systems, DY318-05), DuoSet ELISA Ancillary Reagent Kit 2 (R&D Systems, DY008B), and Human IL-18BP ELISA Kit (abcam, ab100559) according to the manufacturers' instructions.

Tumor treatment studies

Tumor cells were engrafted subcutaneously onto the flanks of 7-9-week-old age-matched male mice. The following number of tumor cells were engrafted per mouse: 0.5 x 10^6 Renca cells; 1.0 x 10^6 RAG cells; and 0.5 x 10^6 YUMMER1.7 cells. Drug treatment was started when the mean tumor size was between 50 and 100 mm^3 (usually at day 7 post engraftment for Renca and YUMMER1.7 tumors, and day 10 for RAG tumors); mice with tumors less than 30 mm^3 or greater than 150 mm^3 at this time were excluded from treatment. The remaining mice were randomized into treatment groups and treated twice weekly for 5 doses for the efficacy studies, and for 3 doses for the cytokine/chemokine and single-cell transcriptomic profiling studies. Antibody treatments were delivered intraperitoneally, and DR-18 was delivered subcutaneously. Drug treatments were diluted in sterile PBS and dosed as follows: anti-PD-1 (clone RMP1-14, BioXCell, BE0146) 200 µg; anti-CTLA-4 (clone 9H10, BioXCell, BE0131) 200 µg for Renca, RAG tumors, and 50 µg for YUMMER1.7 tumors; and DR-18 0.32 mg/kg. Control groups were treated with sterile PBS. Tumor growth was monitored at least twice weekly by caliper measurement. Tumor volumes were calculated as follows: volume = 0.5233 x length x width x height. Mice were euthanized when tumors reached IACUC-approved endpoints (volume greater

than or equal to 1000 mm^3 or ulceration). Survival analyses reflect these endpoints. The investigators were not blinded to the treatment allocation during experiments and outcome assessment.

For the immune cell depletion/effector molecule neutralization studies, depleting/neutralizing antibodies were injected 24 hours prior to each drug treatment (including the first drug treatment), and then twice weekly for the duration of the experiment. The following depleting/neutralizing antibodies were used: anti-CD8a (clone 2.43, BioXCell, BE0061); anti-CD4 (clone GK1.5, BioXCell, BE003-1); anti-IFNγ (clone XMG1.2, BioXCell, BE0055); and for NK cell depletion, anti-Asialo-GM1 (clone Poly21460, BioLegend, 146002). Anti-CD8a, anti-CD4, and anti-IFNγ were given intra-peritoneally at 200 μg/mouse. Anti-Asialo-GM1 was reconstituted in 1 mL PBS, and 50 μL of a 1:2.5 dilution in PBS was given intra-peritoneally.

For tumor rechallenge studies, mice with complete RAG or YUMMER1.7 tumor regression were re-inoculated subcutaneously with twice the initial dose of tumor cells (2.0×10^6 RAG cells; 1.0×10^6 YUMMER1.7 cells) at day 100 post-initial tumor cell engraftment. Tumor growth and survival were monitored twice weekly as above for 60 days, although no tumors grew out on rechallenge.

Mouse cytokine/chemokine profiling

Whole blood was collected retro-orbitally from mice 24 hours after the first treatment, and upon euthanasia 24 hours after the third treatment. Plasma was isolated and cytokine/chemokine profiling was performed using the 31-plex Mouse Cytokine/Chemokine Array from Eve Technologies (MD31).

scRNA-seq sample preparation

Using the same mice as above for cytokine/chemokine profiling, with three mice per treatment group, 24 hours after the third treatment mice were euthanized and tumors were harvested for analysis. Tumors were dissociated by mincing in RPMI + 2% FBS, incubating with 0.1 mg/ml collagenase and DNase I for 30 min at 37ºC, filtering through a 70 μM filter to obtain a single cell suspension. They were then washed with RPMI + 10% FBS and resuspended in RPMI + 20% FBS. For sorting, cells were incubated for 30 min at 4ºC with fluorophore-conjugated antibodies using the following antibodies: anti-CD45 (clone 30-F11, BD Biosciences) and anti-CD3 (clone 17A2, BD Bioscience). Samples were sorted using a BD FACSAriaII into three populations: T cells ($CD45^+$ $CD3^+$); non-T immune cells ($CD45^+$ $CD3^-$); and tumor and stromal cells ($CD45^-$ $CD3^-$). For live/dead staining, AmCyan Kit (Thermo Fisher Scientific) was used. Sorted cells for each subset were counted manually and then combined in a 2:1:1 ratio of T cells:non-T immune cells:tumor and stromal cells, with an equal contribution from each biologic replicate from an experimental condition. Ten thousand cells from each of the mixed sorted samples for each condition were loaded onto the 10x Genomics Chromium System. Library preparation for scRNA-seq and scTCR-seq was performed using the 5' Reagent Kit from 10x Genomics according to the manufacturer's instructions by the Yale Center for Genome Analysis (YCGA) and passed quality control. Libraries were sequenced using an Illumina NovaSeq (one library per lane) at the YCGA.

scRNA-seq analysis

Cellranger was used to align reads to the mouse reference transcriptome (mm10) and to generate cell-by-gene matrices for each sample library. The Seurat package for R v4.3.0 was used to process the matrices and perform downstream analysis. Low quality cells were filtered out that did not meet the following thresholds: : >= 500 nUMI; >= 250 genes; > 0.785 log10GeneperUMI; and < 0.3 mitochondrial gene ratio. Genes expressed in less than 10 cells were also filtered out. Cell cycle scoring was performed using the CellCycleScoring command using mouse gene sets orthologous to previously described human gene sets. Cell cycle factors were regressed out using the "SCTransform" function, and the data were normalized and integrated on the 3000 most variable features. Principal component (PC) scores from the first 40 PCs were used for clustering with the FindClusters command and a resolution of 0.8. Uniform Manifold Approximation and Projection (UMAP) was used for dimensionality reduction. Cell type assignments for each cluster were performed using SingleR (59) and mouse cell reference datasets (and the ZilionisLungData for mouse for the neutrophil subtype analysis (25)) and verified with expression patterns of cell-type defining markers (Supplemental Figure S5C) and examination of the top 10 conserved markers per cluster (from the FindConservedMarkers function). Clusters identified as stressed or dying cells or with clear mixed immune cell populations, which only comprised clusters with a small total number of cells, were removed from further analysis with the Subset command. Gene expression UMAP plots were generated using the FeaturePlot command. Cluster frequencies by experimental condition were normalized to the total number of cells per condition. The top differentially expressed genes comparing a single cluster to all other clusters were computed using the FindAllMarkers function, the data were scaled, and heatmaps of the top differentially expressed genes by adjusted p-value were created from the Pheatmap package and the DoHeatMap function. Dotplots were generated from

DotPlot command. Enhanced Volcano plots were generated from the EnhancedVolcano package. Gene set enrichment analysis was performed using EnrichR. T cells, macrophages/monocytes, and neutrophils were further subsetted and analyzed separately as described above, with additional analysis as below.

T cell subsets were clustered as above but were additionally annotated using ProjecTILS and a reference mouse tumor-infiltrating T cell dataset (60). Milo was used for differential abundance analysis using K nearest neighbor analysis (17), with k=30, d=30, and prop = 0.1 for the buildGraph and makeNhoods functions, d=30 for the calcNhoodDistance function, anti-CTLA-4 treatment status set as a covariate, data was log normalized and aggregated by experimental condition, and automatic grouping of neighborhoods was performed. For T cell subset analysis, max.lfc.delta=1.75 and overlap=5 using the groupNhoods function; for neutrophil subset analysis, max.lfc.delta=1.5 and overlap=0. To compare Neighborhood groups, the findNhodGroupMarkers function was used.

TCR analysis was performed using scRepertoire package (61) and the filtered contig annotations. NicheNet (26) analysis was performed using the mouse ligand-receptor network and ligand-target matrix, the granulocyte clusters set as the "receiver" and the macrophage, monocyte, $CD8^+$, $CD4^+$, Tregs, and NK cell clusters set as the "sender", and lfc_cutoff=0.15. Pseudotime analysis was performed using the Slingshot package, "UMAP" set for dimensionality reduction, and specifying the control condition ("PBS") as the starting point (62).

Analysis of TCGA data

TCGA PanCancer Atlas data was accessed from the cBioPortal (63, 64) and analyzed using the web browser and in R. For PanCancer analysis, RNASeqV2 RSEM processed and normalized

data were used (which corresponds to the rsem.genes.normalized_results file from TCGA). For RCC specific analysis, mRNA expression z-scores were used, with the reference population set to normal samples. Please see the cBioPortal User Guide for more information on the RNA data available. For *IL18BP* analysis with ccRCC, patient samples were dichotomized based on the median mRNA z-score.

Statistical analysis

Statistical analyses were conducted using R v4.2.2 and Prism 9 (GraphPad Software), and the statistical tests as specified in the text and figure legends. Generally, corrected p values < 0.05 were considered significant.

Study Approval:

The patient specimen study protocols were approved by the Institutional Review Board of Yale University and all patients provided written informed consent. Mouse experiments were performed in accordance with IACUC-approved protocols.

Data availability:

Single-cell RNA and TCR sequencing data have been deposited on the public database GEO (accession number GSE279662). Other data are available in the “Supportive data values” XLS file or from the corresponding authors upon request.

Author contributions:

DAS, HMK, AR participated in conceptualization. DAS, HMK, AR, BYL, DAB, MH, and LJ assisted in methodology. DAS, DD, DGS, LZ, LK, JEM, and JH performed investigation. DAS and HMK participated in visualization, funding acquisition, project administration, and writing (original draft and review/editing/revisions). HMK and AR performed supervision.

Acknowledgments:

The authors would like to acknowledge Lori Charette and Yale Pathology Tissue Services for help in constructing YTMA-528. We would also like to acknowledge the Yale Center for Genome Analysis for their assistance in performing library preparation and sequencing for scRNA-seq.

Funding:

National Institutes of Health grant K12CA215110 (DAS and HMK)

National Institutes of Health grant T32 CA233414-02 (DAS, DGS)

National Institutes of Health grant P50 CA121974 (M. Bosenberg and HMK)

National Institutes of Health grant R01 CA227472 (HMK and K. Herold)

National Institutes of Health grant R01 CA269349 (HMK)

National Institutes of Health grant R01 CA269286 (LJ and HMK)

Department of Defense grant KC230193/ HT9425-24-1-0759 (DAS)

Department of Defense grant KC190128/W81XWH-20-1-0882 (DAB)

Department of Defense grant KC220016/ HT9425-23-1-0735 (DAB)

National Institutes of Health/National Cancer Institute grant 1R37CA279822-01 (DAB)

Louis Goodman and Alfred Gilman Yale Scholar Fund (DAB)

National Institutes of Health/National Cancer Institute grant P30CA016359 (Yale Cancer Center – DAS, HMK, DAB)

References

References

1. Motzer RJ, Tannir NM, McDermott DF, Aren Frontera O, Melichar B, Choueiri TK, et al. Nivolumab plus Ipilimumab versus Sunitinib in Advanced Renal-Cell Carcinoma. N Engl J Med. 2018;378(14):1277-90.

2. Rini BI, Plimack ER, Stus V, Gafanov R, Hawkins R, Nosov D, et al. Pembrolizumab plus Axitinib versus Sunitinib for Advanced Renal-Cell Carcinoma. N Engl J Med. 2019;380(12):1116-27.

3. Choueiri TK, Powles T, Burotto M, Escudier B, Bourlon MT, Zurawski B, et al. Nivolumab plus Cabozantinib versus Sunitinib for Advanced Renal-Cell Carcinoma. N Engl J Med. 2021;384(9):829-41.

4. Motzer R, Alekseev B, Rha SY, Porta C, Eto M, Powles T, et al. Lenvatinib plus Pembrolizumab or Everolimus for Advanced Renal Cell Carcinoma. N Engl J Med. 2021;384(14):1289-300.

5. Motzer RJ, Escudier B, McDermott DF, Aren Frontera O, Melichar B, Powles T, et al. Survival outcomes and independent response assessment with nivolumab plus ipilimumab versus sunitinib in patients with advanced renal cell carcinoma: 42-month follow-up of a randomized phase 3 clinical trial. J Immunother Cancer. 2020;8(2).

6. Braun DA, Bakouny Z, Hirsch L, Flippot R, Van Allen EM, Wu CJ, et al. Beyond conventional immune-checkpoint inhibition - novel immunotherapies for renal cell carcinoma. Nat Rev Clin Oncol. 2021;18(4):199-214.

7. Conlon KC, Miljkovic MD, Waldmann TA. Cytokines in the Treatment of Cancer. J Interferon Cytokine Res. 2019;39(1):6-21.

8. Guo L, Junttila IS, Paul WE. Cytokine-induced cytokine production by conventional and innate lymphoid cells. Trends Immunol. 2012;33(12):598-606.

9. Robertson MJ, Mier JW, Logan T, Atkins M, Koon H, Koch KM, et al. Clinical and biological effects of recombinant human interleukin-18 administered by intravenous infusion to patients with advanced cancer. Clin Cancer Res. 2006;12(14 Pt 1):4265-73.

10. Tarhini AA, Millward M, Mainwaring P, Kefford R, Logan T, Pavlick A, et al. A phase 2, randomized study of SB-485232, rhIL-18, in patients with previously untreated metastatic melanoma. Cancer. 2009;115(4):859-68.

11. Dinarello CA, Novick D, Kim S, Kaplanski G. Interleukin-18 and IL-18 binding protein. Front Immunol. 2013;4:289.

12. Zhou T, Damsky W, Weizman OE, McGeary MK, Hartmann KP, Rosen CE, et al. IL-18BP is a secreted immune checkpoint and barrier to IL-18 immunotherapy. Nature. 2020;583(7817):609-14.
13. Schoenfeld DA, Merkin RD, Moutafi M, Martinez S, Adeniran A, Kumar D, et al. Location matters: LAG3 levels are lower in renal cell carcinoma metastatic sites compared to primary tumors, and expression at metastatic sites only may have prognostic importance. Frontiers in Oncology. 2022;12.
14. Schoenfeld DA, Moutafi M, Martinez S, Djureinovic D, Merkin RD, Adeniran A, et al. Immune dysfunction revealed by digital spatial profiling of immuno-oncology markers in progressive stages of renal cell carcinoma and in brain metastases. J Immunother Cancer. 2023;11(8).
15. Klebe RJ, Chen T, Ruddle FH. Controlled production of proliferating somatic cell hybrids. J Cell Biol. 1970;45(1):74-82.
16. Adachi Y, Kamiyama H, Ichikawa K, Fukushima S, Ozawa Y, Yamaguchi S, et al. Inhibition of FGFR Reactivates IFNgamma Signaling in Tumor Cells to Enhance the Combined Antitumor Activity of Lenvatinib with Anti-PD-1 Antibodies. Cancer Res. 2022;82(2):292-306.
17. Dann E, Henderson NC, Teichmann SA, Morgan MD, Marioni JC. Differential abundance testing on single-cell data using k-nearest neighbor graphs. Nat Biotechnol. 2022;40(2):245-53.
18. Ma RY, Black A, Qian BZ. Macrophage diversity in cancer revisited in the era of single-cell omics. Trends Immunol. 2022;43(7):546-63.
19. Biswas SK, Mantovani A. Macrophage plasticity and interaction with lymphocyte subsets: cancer as a paradigm. Nat Immunol. 2010;11(10):889-96.
20. Mantovani A, Allavena P. The interaction of anticancer therapies with tumor-associated macrophages. J Exp Med. 2015;212(4):435-45.
21. Gungabeesoon J, Gort-Freitas NA, Kiss M, Bolli E, Messemaker M, Siwicki M, et al. A neutrophil response linked to tumor control in immunotherapy. Cell. 2023;186(7):1448-64 e20.
22. Hirschhorn D, Budhu S, Kraehenbuehl L, Gigoux M, Schroder D, Chow A, et al. T cell immunotherapies engage neutrophils to eliminate tumor antigen escape variants. Cell. 2023;186(7):1432-47 e17.
23. Salcher S, Sturm G, Horvath L, Untergasser G, Kuempers C, Fotakis G, et al. High-resolution single-cell atlas reveals diversity and plasticity of tissue-resident neutrophils in non-small cell lung cancer. Cancer Cell. 2022;40(12):1503-20 e8.

24. Shaul ME, Fridlender ZG. Tumour-associated neutrophils in patients with cancer. Nat Rev Clin Oncol. 2019;16(10):601-20.

25. Zilionis R, Engblom C, Pfirschke C, Savova V, Zemmour D, Saatcioglu HD, et al. Single-Cell Transcriptomics of Human and Mouse Lung Cancers Reveals Conserved Myeloid Populations across Individuals and Species. Immunity. 2019;50(5):1317-34 e10.

26. Browaeys R, Saelens W, Saeys Y. NicheNet: modeling intercellular communication by linking ligands to target genes. Nat Methods. 2020;17(2):159-62.

27. Hong MMY, Maleki Vareki S. Addressing the Elephant in the Immunotherapy Room: Effector T-Cell Priming versus Depletion of Regulatory T-Cells by Anti-CTLA-4 Therapy. Cancers (Basel). 2022;14(6).

28. Wei SC, Anang NAS, Sharma R, Andrews MC, Reuben A, Levine JH, et al. Combination anti-CTLA-4 plus anti-PD-1 checkpoint blockade utilizes cellular mechanisms partially distinct from monotherapies. Proc Natl Acad Sci U S A. 2019;116(45):22699-709.

29. Wei SC, Duffy CR, Allison JP. Fundamental Mechanisms of Immune Checkpoint Blockade Therapy. Cancer Discov. 2018;8(9):1069-86.

30. Wei SC, Levine JH, Cogdill AP, Zhao Y, Anang NAS, Andrews MC, et al. Distinct Cellular Mechanisms Underlie Anti-CTLA-4 and Anti-PD-1 Checkpoint Blockade. Cell. 2017;170(6):1120-33 e17.

31. Arce Vargas F, Furness AJS, Litchfield K, Joshi K, Rosenthal R, Ghorani E, et al. Fc Effector Function Contributes to the Activity of Human Anti-CTLA-4 Antibodies. Cancer Cell. 2018;33(4):649-63 e4.

32. Peggs KS, Quezada SA, Chambers CA, Korman AJ, Allison JP. Blockade of CTLA-4 on both effector and regulatory T cell compartments contributes to the antitumor activity of anti-CTLA-4 antibodies. J Exp Med. 2009;206(8):1717-25.

33. Quezada SA, Peggs KS. Lost in Translation: Deciphering the Mechanism of Action of Anti-human CTLA-4. Clin Cancer Res. 2019;25(4):1130-2.

34. Sharma A, Subudhi SK, Blando J, Vence L, Wargo J, Allison JP, et al. Anti-CTLA-4 Immunotherapy Does Not Deplete FOXP3(+) Regulatory T Cells (Tregs) in Human Cancers-Response. Clin Cancer Res. 2019;25(11):3469-70.

35. Simpson TR, Li F, Montalvo-Ortiz W, Sepulveda MA, Bergerhoff K, Arce F, et al. Fc-dependent depletion of tumor-infiltrating regulatory T cells co-defines the efficacy of anti-CTLA-4 therapy against melanoma. J Exp Med. 2013;210(9):1695-710.

36. Clark JT, Weizman OE, Aldridge DL, Shallberg LA, Eberhard J, Lanzar Z, et al. IL-18BP mediates the balance between protective and pathological immune responses to Toxoplasma gondii. Cell Rep. 2023;42(3):112147.

37. Menachem A, Alteber Z, Cojocaru G, Fridman Kfir T, Blat D, Leiderman O, et al. Unleashing Natural IL18 Activity Using an Anti-IL18BP Blocker Induces Potent Immune Stimulation and Antitumor Effects. Cancer Immunol Res. 2024:OF1-OF17.

38. Nakamura K, Kassem S, Cleynen A, Chretien ML, Guillerey C, Putz EM, et al. Dysregulated IL-18 Is a Key Driver of Immunosuppression and a Possible Therapeutic Target in the Multiple Myeloma Microenvironment. Cancer Cell. 2018;33(4):634-48 e5.

39. Minnie SA, Waltner OG, Ensbey KS, Nemychenkov NS, Schmidt CR, Bhise SS, et al. Depletion of exhausted alloreactive T cells enables targeting of stem-like memory T cells to generate tumor-specific immunity. Sci Immunol. 2022;7(76):eabo3420.

40. Olivera I, Bolanos E, Gonzalez-Gomariz J, Hervas-Stubbs S, Marino KV, Luri-Rey C, et al. mRNAs encoding IL-12 and a decoy-resistant variant of IL-18 synergize to engineer T cells for efficacious intratumoral adoptive immunotherapy. Cell Rep Med. 2023;4(3):100978.

41. Rappold PM, Vuong L, Leibold J, Chakiryan NH, Curry M, Kuo F, et al. A Targetable Myeloid Inflammatory State Governs Disease Recurrence in Clear-Cell Renal Cell Carcinoma. Cancer Discov. 2022;12(10):2308-29.

42. Auvray M, Auclin E, Barthelemy P, Bono P, Kellokumpu-Lehtinen P, Gross-Goupil M, et al. Second-line targeted therapies after nivolumab-ipilimumab failure in metastatic renal cell carcinoma. Eur J Cancer. 2019;108:33-40.

43. McGregor BA, Lalani AA, Xie W, Steinharter JA, Z EB, Martini DJ, et al. Activity of cabozantinib after immune checkpoint blockade in metastatic clear-cell renal cell carcinoma. Eur J Cancer. 2020;135:203-10.

44. Tannir NM, Agarwal N, Porta C, Lawrence NJ, Motzer R, McGregor B, et al. Efficacy and Safety of Telaglenastat Plus Cabozantinib vs Placebo Plus Cabozantinib in Patients With Advanced Renal Cell Carcinoma: The CANTATA Randomized Clinical Trial. JAMA Oncol. 2022;8(10):1411-8.

45. Ornstein MC, Pal SK, Wood LS, Tomer JM, Hobbs BP, Jia XS, et al. Individualised axitinib regimen for patients with metastatic renal cell carcinoma after treatment with checkpoint inhibitors: a multicentre, single-arm, phase 2 study. Lancet Oncol. 2019;20(10):1386-94.

46. Rini BI, Pal SK, Escudier BJ, Atkins MB, Hutson TE, Porta C, et al. Tivozanib versus sorafenib in patients with advanced renal cell carcinoma (TIVO-3): a phase 3, multicentre, randomised, controlled, open-label study. Lancet Oncol. 2020;21(1):95-104.

47. Wiele AJ, Bathala TK, Hahn AW, Xiao L, Duran M, Ross JA, et al. Lenvatinib with or Without Everolimus in Patients with Metastatic Renal Cell Carcinoma After Immune Checkpoint Inhibitors and Vascular Endothelial Growth Factor Receptor-Tyrosine Kinase Inhibitor Therapies. Oncologist. 2021;26(6):476-82.

48. Pal SK, Albiges L, Tomczak P, Suarez C, Voss MH, de Velasco G, et al. Atezolizumab plus cabozantinib versus cabozantinib monotherapy for patients with renal cell carcinoma after progression with previous immune checkpoint inhibitor treatment (CONTACT-03): a multicentre, randomised, open-label, phase 3 trial. Lancet. 2023;402(10397):185-95.

49. McKay RR, McGregor BA, Xie W, Braun DA, Wei X, Kyriakopoulos CE, et al. Optimized Management of Nivolumab and Ipilimumab in Advanced Renal Cell Carcinoma: A Response-Based Phase II Study (OMNIVORE). J Clin Oncol. 2020;38(36):4240-8.

50. Atkins MB, Jegede OA, Haas NB, McDermott DF, Bilen MA, Stein M, et al. Phase II Study of Nivolumab and Salvage Nivolumab/Ipilimumab in Treatment-Naive Patients With Advanced Clear Cell Renal Cell Carcinoma (HCRN GU16-260-Cohort A). J Clin Oncol. 2022;40(25):2913-23.

51. Grimm MO, Schmitz-Drager BJ, Zimmermann U, Grun CB, Baretton GB, Schmitz M, et al. Tailored Immunotherapy Approach With Nivolumab in Advanced Transitional Cell Carcinoma. J Clin Oncol. 2022;40(19):2128-37.

52. Choueiri TK, Kluger H, George S, Tykodi SS, Kuzel TM, Perets R, et al. FRACTION-RCC: nivolumab plus ipilimumab for advanced renal cell carcinoma after progression on immuno-oncology therapy. J Immunother Cancer. 2022;10(11).

53. Wang J, Perry CJ, Meeth K, Thakral D, Damsky W, Micevic G, et al. UV-induced somatic mutations elicit a functional T cell response in the YUMMER1.7 mouse melanoma model. Pigment Cell Melanoma Res. 2017;30(4):428-35.

54. Baine MK, Turcu G, Zito CR, Adeniran AJ, Camp RL, Chen L, et al. Characterization of tumor infiltrating lymphocytes in paired primary and metastatic renal cell carcinoma specimens. Oncotarget. 2015;6(28):24990-5002.

55. Barr ML, Jilaveanu LB, Camp RL, Adeniran AJ, Kluger HM, Shuch B. PAX-8 expression in renal tumours and distant sites: a useful marker of primary and metastatic renal cell carcinoma? J Clin Pathol. 2015;68(1):12-7.

56. Shuch B, Falbo R, Parisi F, Adeniran A, Kluger Y, Kluger HM, et al. MET Expression in Primary and Metastatic Clear Cell Renal Cell Carcinoma: Implications of Correlative Biomarker Assessment to MET Pathway Inhibitors. Biomed Res Int. 2015;2015:192406.

57. Camp RL, Chung GG, Rimm DL. Automated subcellular localization and quantification of protein expression in tissue microarrays. Nat Med. 2002;8(11):1323-7.

58. Jilaveanu LB, Shuch B, Zito CR, Parisi F, Barr M, Kluger Y, et al. PD-L1 Expression in Clear Cell Renal Cell Carcinoma: An Analysis of Nephrectomy and Sites of Metastases. J Cancer. 2014;5(3):166-72.

59. Aran D, Looney AP, Liu L, Wu E, Fong V, Hsu A, et al. Reference-based analysis of lung single-cell sequencing reveals a transitional profibrotic macrophage. Nat Immunol. 2019;20(2):163-72.

60. Andreatta M, Corria-Osorio J, Muller S, Cubas R, Coukos G, Carmona SJ. Interpretation of T cell states from single-cell transcriptomics data using reference atlases. Nat Commun. 2021;12(1):2965.

61. Borcherding N, Bormann NL, Kraus G. scRepertoire: An R-based toolkit for single-cell immune receptor analysis. F1000Res. 2020;9:47.

62. Street K, Risso D, Fletcher RB, Das D, Ngai J, Yosef N, et al. Slingshot: cell lineage and pseudotime inference for single-cell transcriptomics. BMC Genomics. 2018;19(1):477.

63. Cerami E, Gao J, Dogrusoz U, Gross BE, Sumer SO, Aksoy BA, et al. The cBio cancer genomics portal: an open platform for exploring multidimensional cancer genomics data. Cancer Discov. 2012;2(5):401-4.

64. Gao J, Aksoy BA, Dogrusoz U, Dresdner G, Gross B, Sumer SO, et al. Integrative analysis of complex cancer genomics and clinical profiles using the cBioPortal. Sci Signal. 2013;6(269):pl1.

Figures and Legends

Figure 1

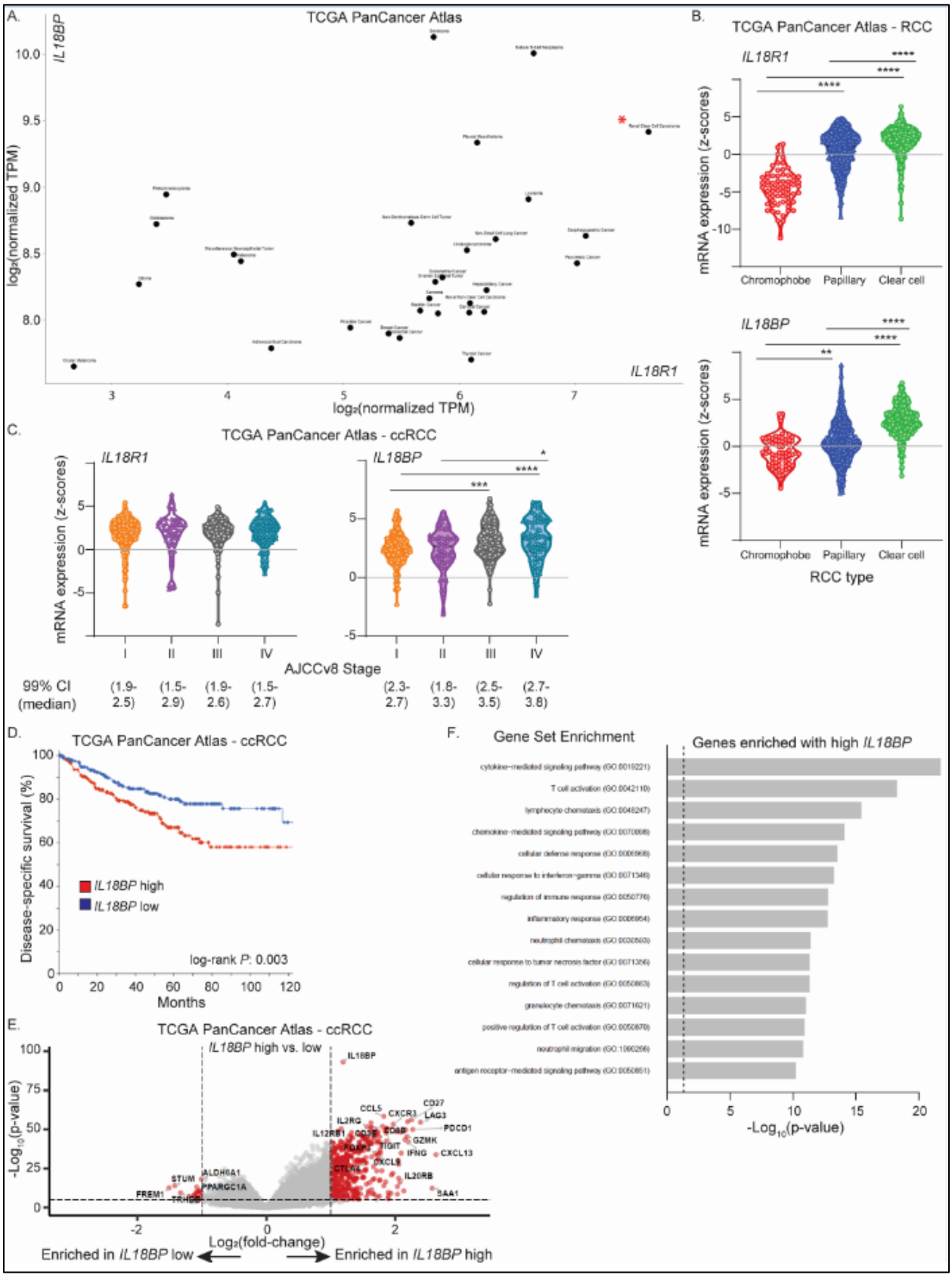
A.
TCGA PanCancer Atlas
IL18BP
IL18R1
log2(normalized TPM)
B.
TCGA PanCancer Atlas - RCC
IL18R1
IL18BP
mRNA expression (z-scores)
Chromophobe
Papillary
Clear cell
RCC type
C.
TCGA PanCancer Atlas - ccRCC
AJCCv8 Stage
99% CI (median)
(1.9-2.5)
(1.5-2.9)
(1.9-2.6)
(1.5-2.7)
(2.3-2.7)
(1.8-3.3)
(2.5-3.5)
(2.7-3.8)
D.
TCGA PanCancer Atlas - ccRCC
Disease-specific survival (%)
IL18BP high
IL18BP low
log-rank P: 0.003
Months
E.
TCGA PanCancer Atlas - ccRCC
IL18BP high vs. low
-Log10(p-value)
Log2(fold-change)
Enriched in IL18BP low
Enriched in IL18BP high
F.
Gene Set Enrichment
Genes enriched with high IL18BP
-Log10(p-value)

Figure 1: *IL18BP* and *IL18R1* are expressed at high levels in ccRCC and elevated *IL18BP* is associated with cytokine and T cell activation and worse survival. *IL18R1* and *IL18BP* expression from TCGA PanCancer Atlas for **(A)** all tumors (ccRCC indicated with red star *), **(B)** RCC histologic subtypes, and **(C)** for ccRCC, by stage. **D.** Kaplan-Meier survival curves based on *IL18BP* expression in ccRCC, dichotomized by median expression. **E.** Volcano plot of transcripts enriched with high versus low *IL18BP* expression in ccRCC (log_2(fold-change) thresholds of 1 and -1; and p-value threshold of 10^{-6}) and **(F)** the top gene sets from enrichment analysis of transcripts enriched with high *IL18BP* expression. For (B-C), statistical testing was performed using Kruskal-Wallis test with Dunn's correction for multiple comparisons. * $P < 0.05$; ** $P < 0.01$; *** $P < 0.001$; **** $P < 0.0001$

1

1

Figure 2

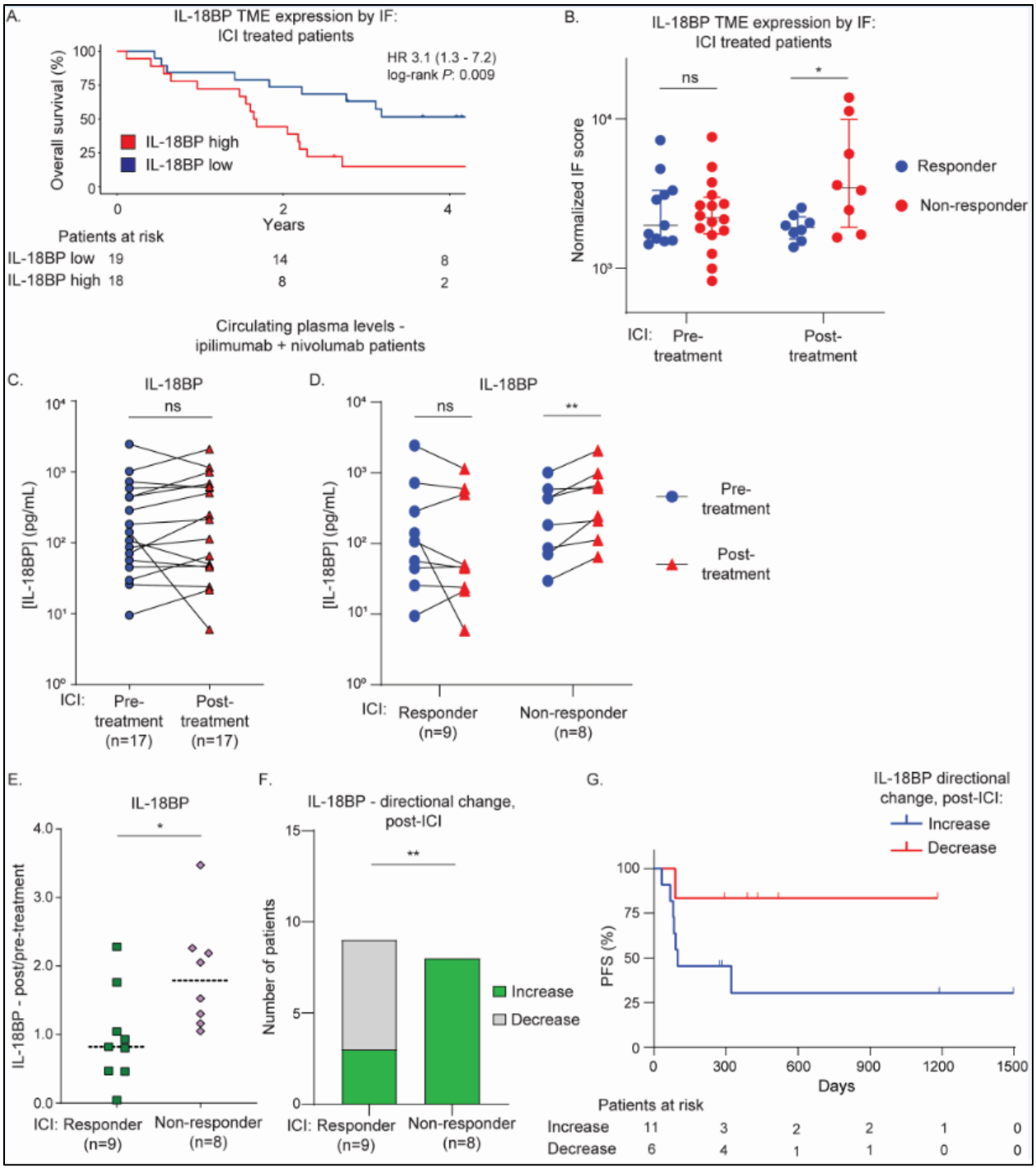
A.
IL-18BP TME expression by IF:
ICI treated patients
HR 3.1 (1.3 - 7.2)
log-rank P: 0.009
Overall survival (%)
IL-18BP high
IL-18BP low
Years
Patients at risk
IL-18BP low 19 14 8
IL-18BP high 18 8 2
B.
IL-18BP TME expression by IF:
ICI treated patients
ns
*
Normalized IF score
Responder
Non-responder
ICI: Pre-treatment Post-treatment
Circulating plasma levels -
ipilimumab + nivolumab patients
C.
IL-18BP
ns
[IL-18BP] (pg/mL)
ICI: Pre-treatment (n=17) Post-treatment (n=17)
D.
IL-18BP
ns
**
Pre-treatment
Post-treatment
ICI: Responder (n=9) Non-responder (n=8)
E.
IL-18BP
*
IL-18BP - post/pre-treatment
ICI: Responder (n=9) Non-responder (n=8)
F.
IL-18BP - directional change, post-ICI
**
Number of patients
Increase
Decrease
ICI: Responder (n=9) Non-responder (n=8)
G.
IL-18BP directional change, post-ICI:
Increase
Decrease
PFS (%)
Days
Patients at risk
Increase 11 3 2 2 1 0
Decrease 6 4 1 1 0 0

Figure 2: IL-18BP protein levels increase post-immunotherapy in non-responding RCC patients. A. Kaplan-Meier curves of overall survival of RCC patients post-ICIs by IL-18BP protein expression, dichotomized by median qIF levels. **B.** IL-18BP protein levels assessed by qIF in the same RCC patient cohort as **(A)**, pre- and post-ICIs, in ICI responders/non-responders. **C.** Circulating plasma levels of IL-18BP, as assessed by ELISA, from patient-matched samples pre- and post- ipi + nivo treatment in a different RCC patient cohort from **(A-B)**. **D.** Circulating plasma levels of IL-18BP from patient-matched samples before- and on- ipi + nivo treatment, separated by treatment response. **E.** The ratio of post/pre-treatment IL-18BP plasma levels by treatment response. **F.** The directional change of IL-18BP plasma levels post-treatment by response. **G.** Kaplan-Meier curves of progression free survival (PFS) post- ipi + nivo by directional change in circulating IL-18BP levels post-treatment, in same RCC cohort as in **(C-F)**. Statistical testing was performed using Mann-Whitney test (B, E), Wilcoxon matched-pairs signed rank test (C-D), and Fisher's exact test (F). Due to small samples sizes, formal statistical testing was not conducted on (G), and the analysis should be viewed as hypothesis-generating. ns = non-significant; * $P < 0.05$; ** $P < 0.01$; *** $P < 0.001$; **** $P < 0.0001$

1

1

Figure 3

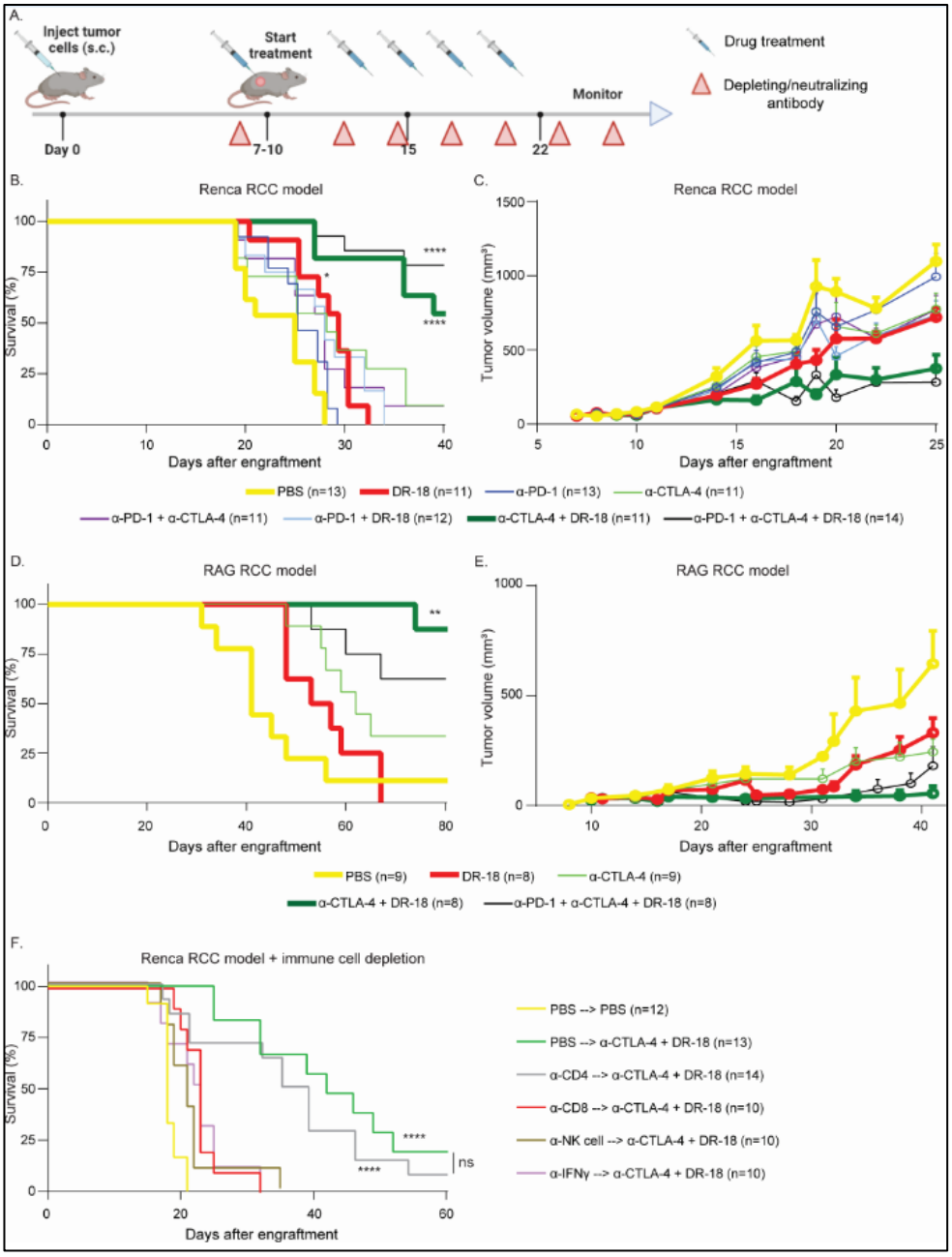

Figure 3: DR-18 combined with anti-CTLA-4 extends survival in murine RCC models. A. Wild-type immunocompetent balb/c mice were subcutaneously (s.c.) engrafted with 0.5 x 10^6 Renca or 1.0 x 10^6 RAG cells. Starting on day 7-10, mice were treated twice weekly with phosphate buffered saline (PBS), DR-18 (s.c.), and/or ICIs (anti-PD-1 / anti-CTLA-4) intraperitoneally. Five treatments were given. Red triangles indicate timing of administration of depleting/neutralizing antibodies, for **(F)**. Kaplan-Meier survival curves and mean tumor growth curves of mice engrafted with Renca **(B-C)** and RAG (select treatment groups shown) **(D-E)** cells (**C, E** - mean +/- standard error of the mean). **F.** Survival of mice engrafted with Renca tumors and treated with control PBS or DR-18 + anti-CTLA-4, either alone (PBS depletion) or with depleting/neutralizing antibodies. Depleting/neutralizing antibodies were given 24 hours prior to treatment, and twice weekly thereafter. NK cells were depleted using anti-Asialo GM1. Renca data combined from 3 independent experiments; RAG from 2 independent experiments. For Kaplan-Meier curves, statistical testing was performed using the log-rank test with Bonferroni correction in comparison to control-treated mice. ns = non-significant; * P < 0.05; ** P < 0.01; *** P < 0.001; **** P < 0.0001

Figure 4

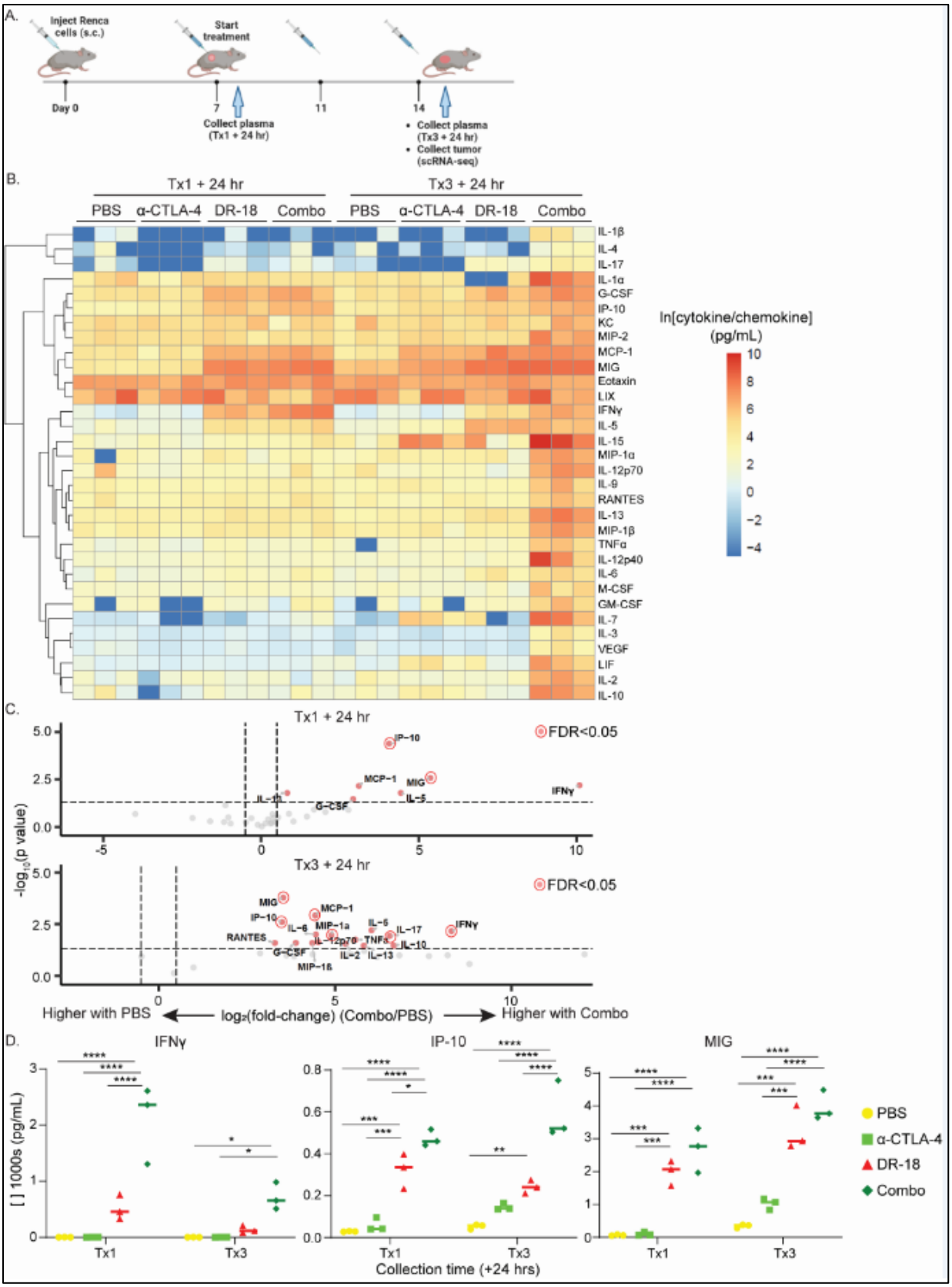
A.
Inject Renca cells (s.c.)
Start treatment
Day 0
7
11
14
Collect plasma (Tx1 + 24 hr)
Collect plasma (Tx3 + 24 hr)
Collect tumor (scRNA-seq)
B.
Tx1 + 24 hr
Tx3 + 24 hr
PBS
α-CTLA-4
DR-18
Combo
IL-1β
IL-4
IL-17
IL-1α
G-CSF
IP-10
KC
MIP-2
MCP-1
MIG
Eotaxin
LIX
IFNγ
IL-5
IL-15
MIP-1α
IL-12p70
IL-9
RANTES
IL-13
MIP-1β
TNFα
IL-12p40
IL-6
M-CSF
GM-CSF
IL-7
IL-3
VEGF
LIF
IL-2
IL-10
ln[cytokine/chemokine] (pg/mL)
10
8
6
4
2
0
−2
−4
C.
Tx1 + 24 hr
FDR<0.05
Tx3 + 24 hr
FDR<0.05
-log10(p value)
Higher with PBS
log2(fold-change) (Combo/PBS)
Higher with Combo
D.
IFNγ
IP-10
MIG
[ ] 1000s (pg/mL)
Tx1
Tx3
Collection time (+24 hrs)
PBS
α-CTLA-4
DR-18
Combo

Figure 4: DR-18 plus anti-CTLA-4 potently induces inflammatory cytokines/chemokines. A. Schematic of treatment and sample collection timepoints for cytokine/chemokine profiling and scRNA/TCR-seq in the Renca model. **B.** Heatmap of the natural logarithm of circulating cytokine/chemokine levels in mice for the indicated treatments and timepoints (n=3 mice/group, with the same mice collected at each timepoint), with unsupervised hierarchical clustering on the y-axis. Data were generated using Eve Technologies' Murine Cytokine Array/Chemokine Array 31-Plex. **C.** Volcano plots of the same data as in **(B)**, comparing circulating cytokine/chemokine levels with DR-18 + anti-CTLA-4 treatment (Combo) to PBS (log_2(fold-change) thresholds of 0.5 and -0.5; and p-value threshold of 0.05; cytokine/chemokine changes with FDR < 0.05 highlighted as indicated) **D.** Absolute levels of the indicated cytokines/chemokines at each timepoint for each treatment. Statistical testing performed using two-way ANOVA with Tukey's multiple comparisons test comparing all conditions within a given timepoint; only significant comparisons are shown. Tx = treatment; hr = hours; s.c. = subcutaneous; scRNA-seq = single-cell RNA sequencing; * P < 0.05; ** P < 0.01; *** P < 0.001; **** P < 0.0001

1

Figure 5

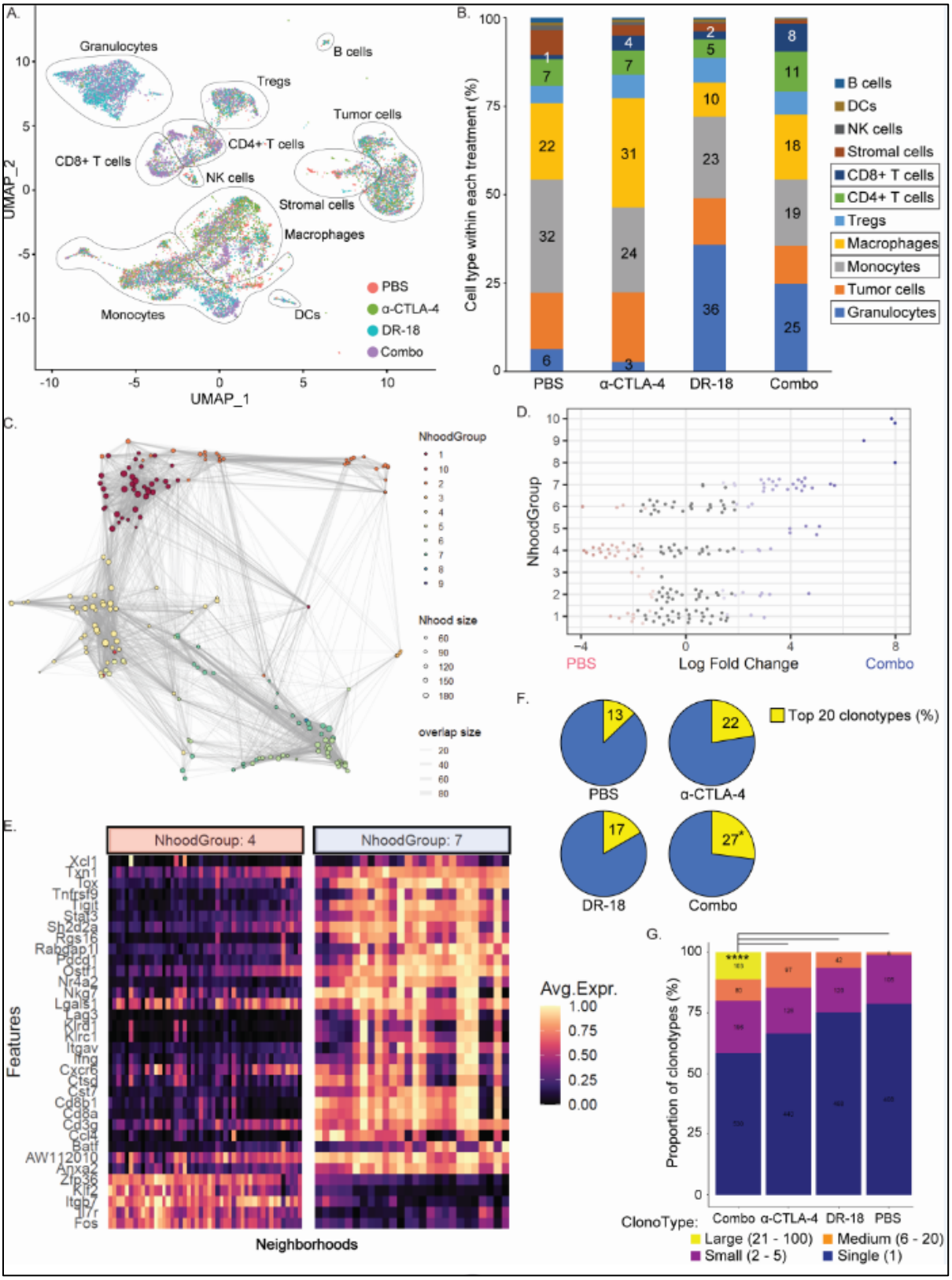
A.
Granulocytes
B cells
Tregs
Tumor cells
CD8+ T cells
CD4+ T cells
NK cells
Stromal cells
Macrophages
Monocytes
DCs
PBS
α-CTLA-4
DR-18
Combo
UMAP_1
UMAP_2
B.
Cell type within each treatment (%)
PBS
α-CTLA-4
DR-18
Combo
B cells
DCs
NK cells
Stromal cells
CD8+ T cells
CD4+ T cells
Tregs
Macrophages
Monocytes
Tumor cells
Granulocytes
C.
NhoodGroup
Nhood size
overlap size
D.
NhoodGroup
PBS
Log Fold Change
Combo
E.
NhoodGroup: 4
NhoodGroup: 7
Features
Neighborhoods
Avg.Expr.
F.
Top 20 clonotypes (%)
PBS
α-CTLA-4
DR-18
Combo
G.
Proportion of clonotypes (%)
ClonoType:
Large (21 - 100)
Medium (6 - 20)
Small (2 - 5)
Single (1)

Figure 5: DR-18 alters immune subset composition in Renca tumors, including enrichment and clonal expansion of $CD8^+$ effector T cells. A. Uniform Manifold Approximation and Projection (UMAP) dimensionality reduction plot of clustering and annotation of all cell populations isolated from Renca tumors treated for three cycles with PBS, DR-18, anti-CTLA-4, or DR-18 + anti-CTLA-4 ("Combo") (n=3 mice/group, pooled) based on scRNA-seq analysis. Annotations were performed using SingleR. **B.** Quantification of the proportion of each cell population from **(A)** within each of the treatment groups, showing enrichment of granulocytes with DR-18 treatment and $CD8^+$ and $CD4^+$ T cells with DR-18 plus anti-CTLA-4. For select cell populations (boxed), the percentages within each treatment group are shown. **C.** Neighborhood group plot from Milo analysis of T cell subsets from scRNA-seq data. **D.** Differential abundance fold changes of the neighborhood groups in **(C)**, comparing the Combo treatment to control, showing enrichment and de-enrichment of certain groups. **E.** Heatmap of the top differentially expressed genes between neighborhood group #7, enriched with DR-18 + anti-CTLA-4 treatment and with high expression levels of markers of T cell activation, cytolytic activity, and exhaustion, versus neighborhood group #4, de-enriched with combination treatment. **F.** Relative proportion of the top 20 clonotypes out of the total for each treatment group based on TCR analysis. **G.** Clonotype proportions by size category based on TCR analysis, showing clonal expansion with DR-18 + anti-CTLA-4 (Combo). Statistical testing performed using Fisher's exact test comparing control to all other treatment conditions, with only significant comparisons shown (F), and Chi-square test comparing DR-18 + anti-CTLA-4 (Combo) to all other conditions. * $P < 0.05$; ** $P < 0.01$; *** $P < 0.001$; **** $P < 0.0001$

1

1

Figure 6

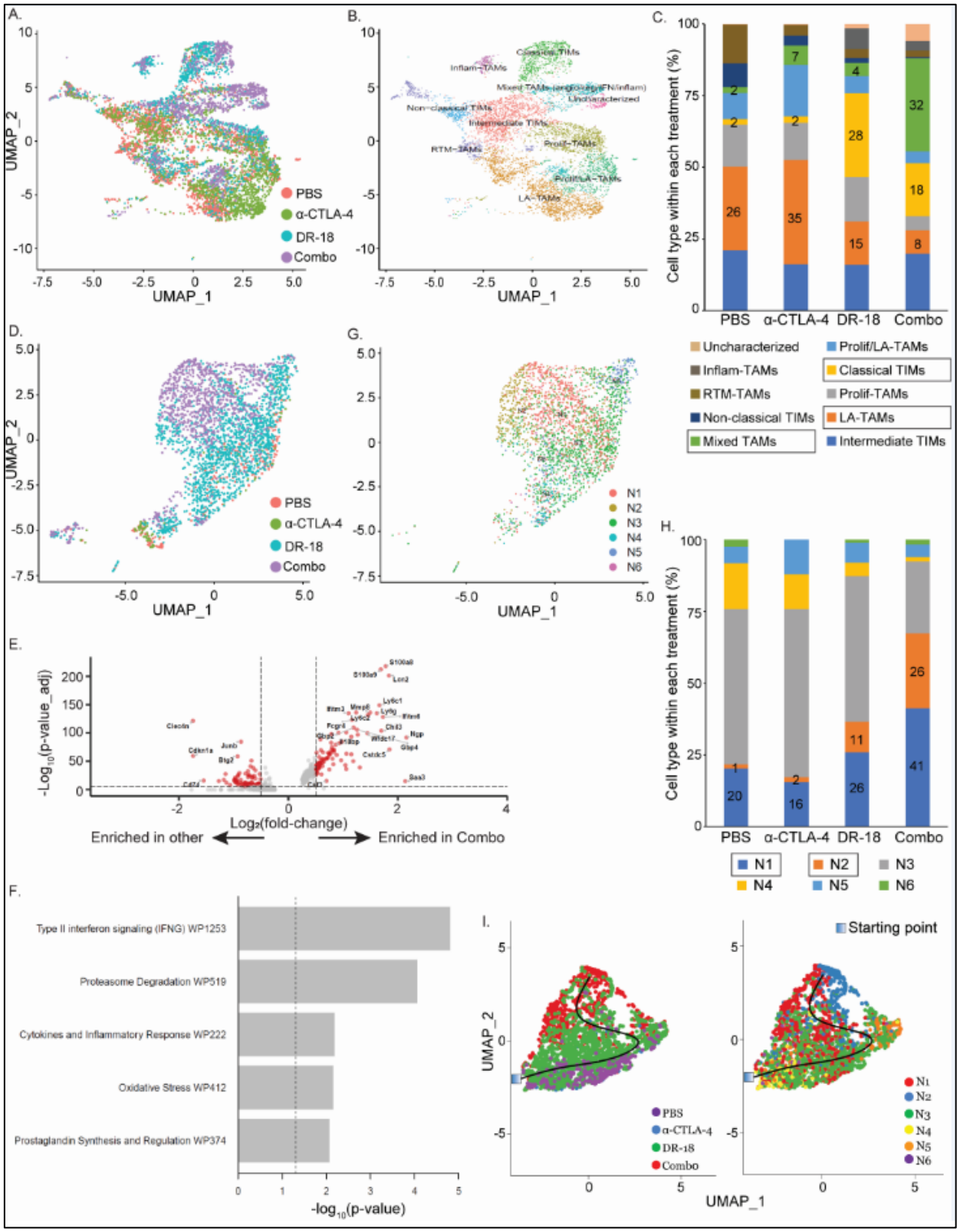
A.
B.
C.
UMAP_2
UMAP_1
PBS
α-CTLA-4
DR-18
Combo
Inflam−TAMs
Non−classical TIMs
Intermediate TIMs
RTM−TAMs
Prolif−TAMs
Prolif/LA−TAMs
LA−TAMs
Uncharacterized
Cell type within each treatment (%)
Uncharacterized
Prolif/LA-TAMs
Inflam-TAMs
Classical TIMs
RTM-TAMs
Prolif-TAMs
Non-classical TIMs
LA-TAMs
Mixed TAMs
Intermediate TIMs
D.
G.
N1
N2
N3
N4
N5
N6
H.
E.
-Log10(p-value_adj)
Log2(fold-change)
Enriched in other
Enriched in Combo
F.
Type II interferon signaling (IFNG) WP1253
Proteasome Degradation WP519
Cytokines and Inflammatory Response WP222
Oxidative Stress WP412
Prostaglandin Synthesis and Regulation WP374
-log10(p-value)
I.
Starting point

Figure 6: DR-18 plus anti-CTLA-4 leads to intra-tumoral expansion of pro-inflammatory myeloid populations. UMAP plots of all macrophages/monocytes identified by scRNA-seq analysis with overlaid **(A)** treatment groups and **(B)** annotated clusters. Annotation was performed based on the phenotypic groups and markers described in Ma *et al*. **C.** Quantification of the proportion of each macrophage/monocyte subtype from **(B)** within each of the treatment groups, showing relative enrichment of pro-inflammatory and loss of pro-tumorigenic subtypes. For select cell populations (boxed), the percentages within each treatment group are shown. **D.** UMAP plot of all granulocytes identified by scRNA-seq analysis with overlaid treatment groups. **E.** Volcano plot of differential gene expression between granulocytes from tumors treated with combination DR-18 + anti-CTLA-4 (Combo) versus all other treatment groups (Other) (log_2(fold-change) thresholds of 0.5 and -0.5; and p-value-adjusted threshold of 10^{-6}). **F.** The top gene sets from enrichment analysis of genes enriched in granulocytes from Combo-treated tumors. **G.** UMAP plot of all neutrophils from scRNA-seq analysis with overlaid neutrophil subtype classification based on Zilionis *et al*, with **(H)** quantification of the relative proportion of each subtype by treatment group. For select cell populations (boxed), the percentages within each treatment group are shown. **I.** UMAP plots of neutrophils showing trajectory analysis using Slingshot from the given starting point, with overlaid treatment groups (left) and neutrophil subtypes (right), as in **(G)**.